

Deep-subwavelength single grooves prepared by femtosecond laser direct writing on Si

Rui-Xi Ye(叶瑞熙) and Min Huang(黄敏)

Citation: Chin. Phys. B, 2024, 33 (**8**): 087901. DOI: 10.1088/1674-1056/ad4cd6

What follows is a list of articles you may be interested in

Subpicosecond laser ablation behavior of a magnesium target and crater evolution: Molecular dynamics study and experimental validation

Guolong Jiang(江国龙) and Xia Zhou(周霞)
Chin. Phys. B, 2024, 33 (**7**): 077901. DOI: 10.1088/1674-1056/ad3ef8

Laser fragmentation in liquid synthesis of novel palladium-sulfur compound nanoparticles as efficient electrocatalysts for hydrogen evolution reaction

Guo-Shuai Fu(付国帅), Hong-Zhi Gao(高宏志), Guo-Wei Yang(杨国伟), Peng Yu(于鹏), and Pu Liu(刘璞)
Chin. Phys. B, 2022, 31 (**7**): 077901. DOI: 10.1088/1674-1056/ac4e0e

Time-resolved shadowgraphs and morphology analyses of aluminum ablation with multiple femtosecond laser pulses

Zehua Wu(吴泽华), Nan Zhang(张楠), Xiaonong Zhu(朱晓农), Liqun An(安力群), Gangzhi Wang(王刚志), Ming Tan(谭明)
Chin. Phys. B, 2018, 27 (**7**): 077901. DOI: 10.1088/1674-1056/27/7/077901

Self-organized voids revisited： Experimental verification of the formation mechanism

Song Juan (宋娟), Ye Jun-Yi (叶俊毅), Qian Meng-Di (钱梦迪), Luo Fang-Fang (骆芳芳), Lin Xian (林贤), Bian Hua-Dong (卞华栋), Dai Ye (戴晔), Ma Guo-Hong (马国宏), Chen Qing-Xi (陈庆希), Jiang Yan (姜燕), Zhao Quan-Zhong (赵全忠), Qiu Jian-Rong (邱建荣)
Chin. Phys. B, 2014, 23 (**7**): 077901. DOI: 10.1088/1674-1056/23/7/077901

Suppressing the mechanical quadrature error of a quartz double-H gyroscope through laser trimming

Zhao Ke (赵克), Feng Li-Hui (冯立辉), Wang Qian-Qian (王茜蒨), Liu Ming-Zhi (刘明智), Wang Ben-Guo (王本国), Cui Fang (崔芳), Sun Yu-Nan (孙雨南)
Chin. Phys. B, 2013, 22 (**11**): 117901. DOI: 10.1088/1674-1056/22/11/117901

RAPID COMMUNICATION

Deep-subwavelength single grooves prepared by femtosecond laser direct writing on Si

Rui-Xi Ye(叶瑞熙) and Min Huang(黄敏)[†]

State Key Laboratory of Optoelectronic Materials and Technologies, School of Physics, Sun Yat-sen University, Guangzhou 510275, *China*

(Received 7 March 2024; revised manuscript received 16 May 2024; accepted manuscript online 17 May 2024)

It is well known that femtosecond laser pulses can easily spontaneously induce deep-subwavelength periodic surface structures on transparent dielectrics but not on non-transparent semiconductors. Nevertheless, in this study, we demonstrate that using high-numerical-aperture 800 nm femtosecond laser direct writing with controlled pulse energy and scanning speed in the near-damage-threshold regime, polarization-dependent deep-subwavelength single grooves with linewidths of $\sim$ 180 nm can be controllably prepared on Si. Generally, the single-groove linewidth increases slightly with increase in the pulse energy and decrease in the scanning speed, whereas the single-groove depth significantly increases from $\sim$ 300 nm to $\sim$ 600 nm with decrease in the scanning speed, or even to over 1 μm with multi-processing, indicating the characteristics of transverse clamping and longitudinal growth of such deep-subwavelength single grooves. Energy dispersive spectroscopy composition analysis of the near-groove region confirms that single-groove formation tends to be an ultrafast, non-thermal ablation process, and the oxidized deposits near the grooves are easy to clean up. Furthermore, the results, showing both the strong dependence of groove orientation on laser polarization and the occurrence of double-groove structures due to the interference of pre-formed orthogonal grooves, indicate that the extraordinary field enhancement of strong polarization sensitivity in the deep-subwavelength groove plays an important role in single-groove growth with high stability and collimation.

Keywords: femtosecond-laser direct writing of Si, deep-subwavelength single grooves, polarization dependence, high numerical aperture, ultrafast non-thermal ablation

PACS: 79.20.Eb, 42.62.–b, 52.38.Mf, 81.15.Fg **DOI:** 10.1088/1674-1056/ad4cd6

1. Introduction

As a cutting-edge material processing tool, femtosecond (fs) lasers with ultra-high peak power can induce high-order nonlinear laser–matter interactions, such as multiphoton and tunneling ionization[1] for which the relevant timescale is much smaller than the thermal conduction time of materials, and can effectively suppress thermal diffusion,[2,3] significantly improving processing accuracy.[2–4] Essentially, fs laser irradiation, as a unique method of transferring light field energy to the irradiated material, can cause extremely high temperatures and pressures as well as strong interaction and energy coupling between the light field and the excited surface, resulting in material surface modification or structural change under these extreme conditions.[5–12] An example is the classic phenomenon of laser-induced periodic surface structures (LIPSS) on solids discovered as early as the 1960s.[6] In the past two decades, with the widespread application of fs lasers in processing, our understanding of LIPSS has become more and more profound. Although LIPSS have complex morphology and formation mechanisms,[6–10] they can be basically divided into low spatial frequency LIPSS (LSFL) and high spatial frequency LIPSS (HSFL).[10–14] LIPSS with different sizes and features can serve as a convenient way to obtain material modification and regular patterning of solids for functionalization, such as structural color, super hydrophobicity, microfluidics, etc.[15–20] Based on various technical methods, such as beam shaping, light field modulation, sample pretreatment, composite processing, etc., large-area preparation of LIPSS can be optimized to improve structural uniformity, processing efficiency and structural diversity.[21–26]

Interestingly, LIPSS with subwavelength or even deep-subwavelength feature sizes demonstrate the ability of laser processing to break the diffraction limit. In particular, for various solids, surface plasma polaritons (SPPs) excited by the incident laser[11] and the resulting extraordinary field enhancement[7] responsible for the scaling down of LIPSS apertures have provided the physical basis for deep-subwavelength processing. Typically, the ultra-high peak power and ultra-short pulse duration of fs lasers provide the physical conditions that favor HSFL formation on dielectrics: the huge field enhancement and the almost instantaneous response of strong-field ionization at nano-apertures[7] can raise ultrafast non-thermal interactions between the excited high-energy electrons and ions, resulting in Coulomb explosion at the nanoscale and thus structures with characteristic sizes far smaller than the optical diffraction limit.

Remarkably, by precisely controlling the fs laser processing conditions, single deep-subwavelength structures derived

[†]Corresponding author. E-mail: syshm@163.com

© 2024 Chinese Physical Society and IOP Publishing Ltd

from LIPSS can be induced in or on dielectrics, such as a single nano-channel in silicate glass,[27] a single nano-groove on titanium oxide[28] and a single nano-slit in silica glass.[29] However, on semiconductors the difficulty of obtaining such single deep-subwavelength structures based on LIPSS is significantly increased, since the stronger thermal effects of semiconductors occurring during laser processing would hinder the formation of regular deep-subwavelength structures. Essentially, non-transparent semiconductors and metals with strong absorption characteristics produce significantly stronger thermal effects than transparent dielectrics during strong fs laser irradiation, which makes them show fs laser processing characteristics and morphological features that differ greatly from dielectrics — they often present more prominent thermal effects, for example larger melting zones caused by the long-term thermal process, which would suppress the ultrafast non-thermal ablation mechanisms of Coulomb explosion and phase explosion[30–32] and hinder the feature size of the formed apertures to reach the near 100 nm level. As a result, on semiconductors the possibility of stable feedback growth of a single deep-subwavelength groove based on LIPSS would be greatly reduced, even in fs laser processing.

Nowadays, although using a processing setup of orthogonally polarized double fs or ns laser beams, grooves of $\sim$ 10 nm[33] or cracks of $\sim$ 30 nm[34] can be formed directly on silicon (Si), single nano-grooves fabricated by single fs laser beam direct writing on Si is still a challenging research topic that requires further experimental exploration. In this paper, by using high-numerical-aperture (NA) objective lenses and precisely controlling the processing conditions of pulse energy and scanning speed, polarization-dependent single-groove structures with a linewidth of $\sim$ 180 nm can be stably prepared on Si by single fs laser beam direct writing. Profiting from the extraordinary field enhancement of polarization dependence in the nano-groove, a uniform nano-groove can grow along an extremely straight line with little influence from laser spot jitter during the scanning processing, and it can also be efficiently deepened by increasing the imposed pulse number or through multi-processing. These results indicate that even on non-transparent Si, single nano-grooves derived from LIPSS can be robustly fabricated via single fs laser beam direct writing, resembling those on dielectrics; this may serve as a convenient nano-processing technique on semiconductors.

2. Materials and methods

2.1. Materials

The experimental samples are optically polished slices of intrinsic high-resistance silicon (Lijing Optoelectronics, crystal orientation $\langle 100 \rangle$, resistivity > 4000 Ω·cm, thickness 0.28 mm). Before laser processing, the sample surface is ultrasonically cleaned in anhydrous ethanol or wiped with mirror wiping paper dipped in anhydrous ethanol to remove surface pollutants. After laser processing, the treated sample may also be ultrasonically cleaned in anhydrous ethanol or wiped with mirror wiping paper dipped in anhydrous ethanol to remove the surface deposits arising during processing.

2.2. Fs laser processing

As shown in Fig. 1(a), the ultra-short pulse output from the Ti:sapphire fs laser (COHERENT, Legend Elite USP HE+), with a wavelength of 800 nm, pulse duration of $\sim$ 50 fs ($\sim$ 600 fs and $\sim$ 1 ps obtained by adjusting the amplifier compressed grating) and repetition rate of 1 kHz, is controlled by switching the optical path on and off using a mechanical shutter, reducing the beam radius through a telescope system and adjusting the pulse energy with a half-wave plate and a Glan prism. Then, the fs laser pulses are reflected into a microscope objective with an NA of 0.95 (Nikon, CF Plan, $100\times/0.95$, working distance 0.3 mm) or 0.5 (Mitutoyo, M Plan APO SL, $80\times/0.5$, working distance 15 mm) to converge and irradiate on the sample surface. Microscope objectives with lower NA have also been used in the attempt to prepare deep-subwavelength single grooves, but the experimental results indicate that it is quite difficult to induce stable deep-subwavelength single grooves using objectives with an NA of 0.4 or lower, as shown by the results in Fig. S5 of the supplementary information. Due to the dispersion effect of the microscope objective, the pulse duration will undergo a certain degree of broadening after passing through the objective. For example, ultrashort pulses with a duration of 58 fs will widen to 74 fs after passing through the 0.95 NA Nikon objective, as demonstrated by the result in Fig. S6 of the supplementary information. Considering that the pulse duration does not show very significant broadening, it can be assumed that within the pulse duration regime of $\sim$ 50 fs used in our experiment the objective does not significantly alter the characteristics of the ultrashort pulses.

The sample is placed on a high-precision three-dimensional (XYZ axis) displacement stage (Newport, two XMS50 stages for the X and Y directions, one VP-5ZA stage for the Z direction, minimum incremental motion of 10 nm) to achieve high-precision three-dimensional displacement of the sample. The objective lens is also equipped with an ultra-high-precision Z-axis piezoelectric motion module (Newport, NPO140SG-D, minimum incremental motion of 1 nm) to precisely control focusing. These four motion axes are controlled by a universal multi-axis high-precision motion controller (Newport, XPS-Q8). At the same time, the real-time processing status of the sample surface is imaged on a color digital camera through a coaxial microscopic imaging system (equipped with a white light coaxial illumination source). In fs laser processing, to achieve single-groove processing the sin-

gle pulse energy should be precisely controlled near the damage threshold. Therefore, precise measurement of the laser pulse energy is crucial. Actually, in this study the pulse energy in the nJ range is not directly measured by a laser energy meter but derived from the average laser power measured by a power meter (Thorlabs, PM series) divided by the laser pulse repetition rate (1 kHz), which has also been corrected for the influence of objective transmittance. Through such an indirect measurement method we can obtain accurate measurements of nJ level pulse energy, as shown in Fig. S7 of the supplementary information.

2.3. Characterization techniques

The morphological characteristics of the treated samples are analyzed using a scanning electron microscope (SEM) (Carl Zeiss, Auriga-4523) with the SE2 detector (more sensitive to the structural depth information) or in-lens detector (more sensitive to the structural surface information) and SEM (FEI, Quanta 400F). In addition, an SEM (Hitachi, Regulus 8230) equipped with energy dispersive spectroscopy (EDS; Bruker) is used to obtain EDS of structured regions of treated samples for composition analysis via the O and Si component distribution maps.

3. Results and discussion

3.1. The basic technique of preparing a single groove from LIPSS on Si

Figure 1(a) schematically shows the fs laser (800 nm, 50 fs, 1 kHz) processing system and the basic technique of preparing a single groove from LIPSS. As shown by the SEM morphologies, under near-damage-threshold irradiation conditions, LSFL perpendicular to the laser polarization, originating from SPP excitation,[11] can be formed on Si with a groove period of about 500 nm. Thus, by setting the scanning direction perpendicular to the laser polarization and precisely controlling the pulse energy, scanning speed and focusing position, a single-groove structure with a linewidth of $\sim$ 180 nm can be obtained with 800-nm fs laser direct writing with a 0.50 NA objective lens. In detail, firstly, via accurate focusing of the objective, the waist of the converging laser beam is placed on the Si surface, thus achieving the smallest processing spot. Then, by setting the polarization direction perpendicular to the laser scanning direction, LSFL parallel to the scanning direction can be obtained. Finally, based on the definite threshold of fs laser-induced damage, by precisely reducing the laser irradiation intensity the area of laser damage can be restricted to only one groove of the LIPSS (the radius of the damaged area is smaller than the ripple period Λ_{SPP} of the LSFL), thus achieving single-groove processing, as shown by the sketch maps below the SEM images. Interestingly, compared with the double nano-grooves, the single nano-groove appears more linear and uniform, demonstrating more stable incubation growth of the single nano-groove benefiting from the more stable field enhancement mode of a single nano-groove rather than the symmetric or asymmetric field enhancement modes of two adjacent nano-grooves with more possibilities for mode switching.[7,12] In addition, the ablation deposits of adjacent grooves are also prone to mutual interference with stable growth of grooves.

It can be revealed that towards the single grooves on Si the linewidth of $\sim$ 180 nm is significantly larger than those of several tens of nm reported in dielectrics.[27–29] Note that the significantly different linewidths originate from the different origins of the single grooves in Si and dielectrics: here for Si the single grooves originate from LSFL, which have typical structural feature sizes greater than 100 nm while for dielectrics the single grooves originate from HSFL, which have typical structural feature sizes smaller than 100 nm. Essentially, the formation of a larger laser-induced single-aperture size for Si is due to the stronger thermal effects exhibited by semiconductors during laser processing, which leads to a larger heat conduction distance and thus a larger thermal affected area. Therefore, in fs laser processing the ultimate single-aperture size in Si is much larger than that in dielectrics.

3.2. Variation of line width and line depth as functions of pulse energy and scanning speed

Under appropriate high-NA focusing conditions of fs laser irradiation, single-groove structures can be prepared in a suitable processing parameter window determined by the pulse energy and the scanning speed (Fig. S1 in the supplementary information presents the processing window for single grooves by sweeping more comprehensive parameters with wider ranges, including pulse width and focusing NA). Figures 1(b) and 1(c) show the variation of groove linewidth as a function of pulse energy and scanning speed, respectively, under 800 nm fs laser irradiation with a 0.95 NA objective lens. In Fig. 1(b), with a scanning speed of 10 $\mu m \cdot s^{-1}$, the linewidth will increase slightly from $\sim$ 180 nm to $\sim$ 220 nm as the pulse energy increases from 1.24 nJ to 1.48 nJ, with the melt-modified region around the groove becoming somewhat more significant (Fig. S2(a) in the supplementary information shows the linewidth variation in a wider pulse-energy range). In Fig. 1(c), with a pulse energy of 1.24 nJ, double-groove structures with a linewidth over 600 nm are induced when the scanning speed is in the low-value range between 1 $\mu m \cdot s^{-1}$ and 4 $\mu m \cdot s^{-1}$; this can be clearly seen in the corresponding side view of Fig. 2(b). This means that the strong thermal accumulation and excessive feedback towards too high an effective pulse number resulting in the occurrence of double grooves would cause the structure linewidth to increase significantly near the LSFL period related to SPP wavelength. Then, when

the scanning speed increases from 6 μm·s^{-1} to 40 μm·s^{-1}, the single groove is stably formed as the linewidth decreases from ∼ 220 nm to ∼ 170 nm. Note that with the scanning speed in the high-value range of 10 μm·s^{-1} to 40 μm·s^{-1}, the linewidth tends to stabilize and no longer decreases but the uniformity, linearity or even continuity of the single groove seems to become worse due to the insufficient feedback towards too low an effective pulse number that is unable to provide sufficient incubation effect for the stable growth of the single groove. A similar trend of scanning-speed dependence for the single-groove linewidth was also observed in another set of results shown in Fig. S2(b) in the supplementary information, where double-groove structures do not appear. On the other hand, it can be revealed that for the single groove derived from 800 nm fs laser-induced LSFL on Si, the limit linewidth determined by the ultrafast ablation characteristics of Si is near 170 nm, which is significantly larger than that on dielectrics[27–29] and closely related to the intrinsic physical properties of Si as a typical semiconductor, such as higher absorption rate, electron mobility and thermal conductivity.

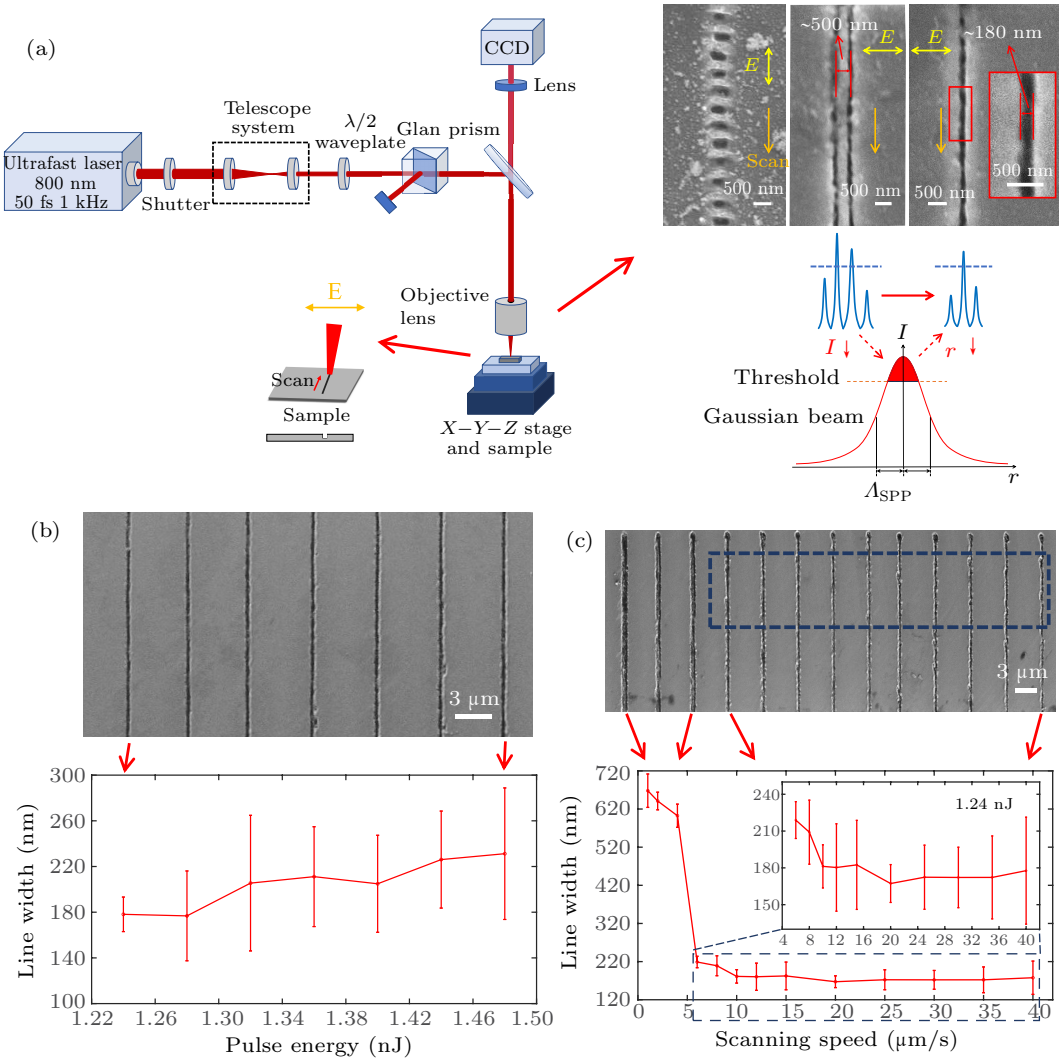


Fig. 1. (a) Schematic diagram of the fs laser (800 nm, 50 fs, 1 kHz) processing system and the basic technique of preparing a single groove from LIPSS. SEM images assisted by the sketch maps on the right side demonstrate the processing technique for obtaining a single groove on Si. The structures in the three SEM images are prepared with an objective lens of NA 0.50, a scanning speed of 10 μm·s^{-1} and pulse energies of 2.73 nJ, 2.73 nJ (∼ 1 μm defocus) and 2.20 nJ, respectively. (b) The variation of groove linewidth as a function of pulse energy, with the SEM (SE2) image showing the corresponding single grooves on the wiped surface of Si prepared with an objective lens of NA 0.95, a scanning speed of 10 μm·s^{-1} and pulse energies of 1.24–1.48 nJ (from left to right). (c) The variation of groove linewidth as a function of scanning speed, with the SEM (SE2) image showing the corresponding single grooves on the wiped surface of Si prepared with an objective lens of NA 0.95, a pulse energy of 1.24 nJ, and scanning speeds of 1–40 μm·s^{-1} (from left to right). The red arrows in (b) and (c) mark the correspondence between the scanning line and the data point.

Using scanning processing penetrating perpendicularly through the natural cleavage side of the Si wafer, the cross-sectional profile of a single groove can be clearly revealed by the side SEM observations shown in Fig. 2. In detail, in Fig. 2(a), corresponding to the side view of Fig. 1(b), towards a scanning speed of 10 μm·s^{-1}, the line depth of the single groove varies slightly between ∼ 480 nm and ∼ 500 nm for pulse energy increasing from 1.24 nJ to 1.48 nJ. In Fig. 2(b), for the side view of Fig. 1(c) concerning a pulse energy of 1.24 nJ, the line depth decreases from ∼ 800 nm to ∼ 300 nm

as the scanning speed increases from 1 μm·s^{-1}to 40 μm·s^{-1}, presenting a significant change. Note that with the scanning speed in the range 1–4 μm·s^{-1} the formed structure is a double-groove structure, and in the range 6–40 μm·s^{-1} the formed structure is a single-groove structure with line depth varying between ∼ 600 nm and ∼ 300 nm, still a large change. Considering the almost stable linewidth in the 10–40 μm·s^{-1} range shown in Fig. 1(c), our result confirms that a single nano-groove can be significantly deepened via multi-pulse feedback, growing along the groove while keeping the groove width basically unchanged. In short, such deep-subwavelength single grooves are provided with the characteristics of transverse clamping and longitudinal growth, which should originate from the propagation characteristic of the field-enhancement mode in the deep-subwavelength groove. However, here the excessive effective pulse number will cause the appearance of double-groove structures, which disrupts the further deepening growth of single grooves — actually, using the lower (0.50) NA objective lens with a larger depth of focus, multi-processing by repeating scanning or adjusting the focus position in multi-processing, the single groove can be further deepened, with the depth easily exceeding 1 μm, as shown in Fig. S3 in the supplementary information. Note that compared with the 0.95 NA focusing condition, the 0.50 NA focusing condition with a larger focal spot and pulse energy will cause more severe thermal effects, resulting in clear protrusion of the melting layer next to the groove.

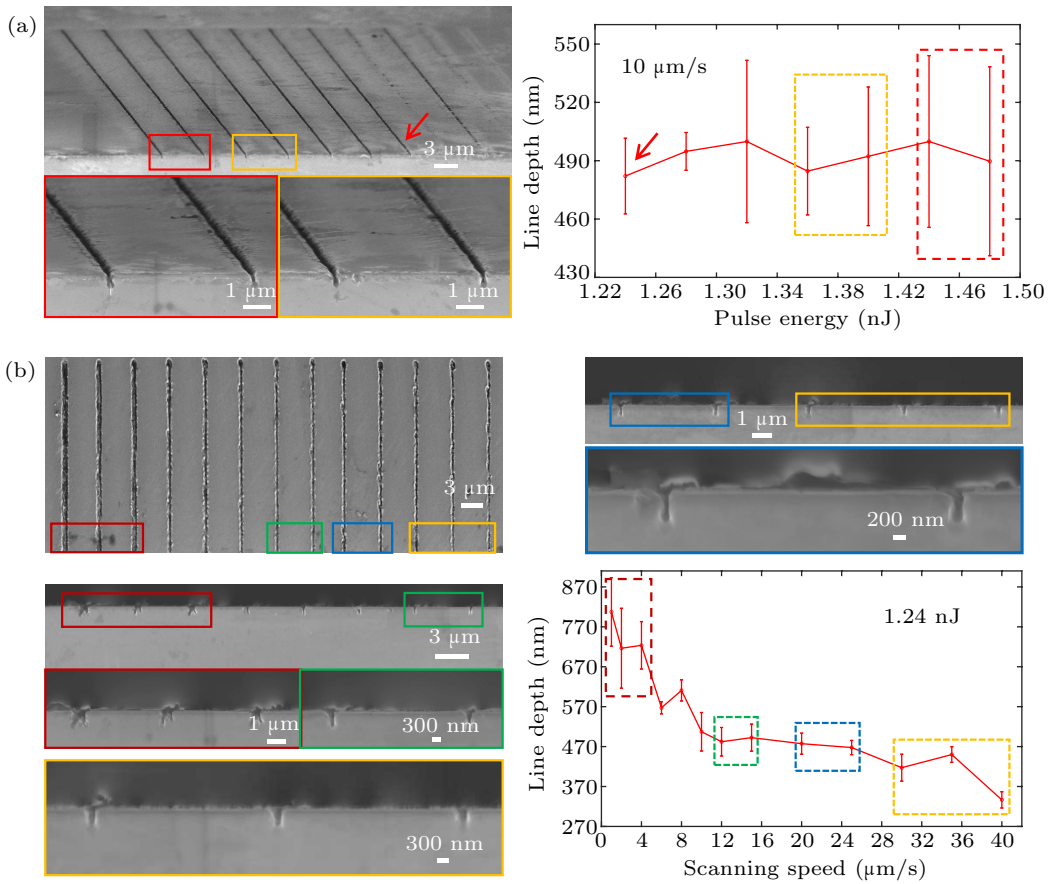


Fig. 2. SEM images of side views of the single-groove structures on the wiped surface of Si prepared by different (a) pulse energies and (b) scanning speeds, with the corresponding variation curve of groove line depth measured from the cross-sectional profile. The processing parameters for the two sets of results are as follows: (a) objective lens of NA 0.95, scanning speed 10 μm·s^{-1}, pulse energies of 1.24–1.48 nJ (from right to left); (b) objective lens of NA 0.95, pulse energy 1.24 nJ, scanning speeds 1–40 μm·s^{-1} (from left to right). The color boxes mark the corresponding regions on the SEM images of the front view, side view and enlarged side view, and the corresponding data in the line-depth curve. The arrows in (a) mark the correspondence between the scanning line and the first data point.

3.3. Energy dispersive spectroscopy measurements near the single groove

EDS measurements focusing on the material composition of the processing area are carried out to obtain information on the mechanisms of single-groove formation. As shown in the SEM image of Fig. 3(a), the nearby areas of four neatly arranged single nano-grooves on the unwiped surface of Si prepared under processing conditions of NA 0.95, 10 μm·s^{-1} and 1.24 nJ are covered with the white deposits that erupted during processing. Then, through the EDS composition analysis of the near-groove region marked by the orange box, as detailed in the enlarged SEM image and the O and Si component distribution maps on the right, it can be revealed that the nano-groove region has a low O content and a high Si content, while the white deposits near the nano-groove show a high O content and low Si content. In particular, inside the nano-

groove, the O content is very low, indicating the occurrence of an ultrafast, non-thermal ablation process in the region. As a result, the high-temperature plume caused by the intense eruptive process with high chemical activity tends to combine with oxygen in the air and deposits near the nano-grooves as oxides. These results confirm that ultrafast Coulomb explosion or phase explosion in the nano-groove removes most of the laser-deposited energy,[32] and thus the thermal effect is correspondingly greatly reduced (without oxidation occurring in the groove). In addition, Fig. 3(b) shows the different structures induced by different scanning speeds and processing times, exhibiting morphological evolution from a molten-pool-filled nano-groove to an ablated hollow nano-groove. In detail, for a single high-speed scanning at a low pulse energy of 1.00 nJ, the multi-pulse incubation effect is still not able to trigger an intense ultrafast ablation process but induces the formation of a molten-pool-filled nano-groove (the right line) owing to thermal accumulation; then, by reducing the scanning speed and increasing the scanning time, ultrafast ablation can be triggered for sufficiently strong multi-pulse incubation, leading to the formation of a hollow single nano-groove (the left line). Towards the molten-pool groove, the composition analysis chart on the right shows no obvious difference between the treated and untreated regions, indicating no special change in the composition during the melting process, which is distinct from the ablation process of the hollow groove presented above. Interestingly, however, here the surface deposits near the molten-pool groove have been partially wiped by cleaning with mirror wiping paper, leaving the melt-recast amorphous silicon with a clear, darker presentation due to a lower electron emission rate than single-crystal silicon (i.e., the ablation deposits causing surface pollution can be easily cleared, as also confirmed by the SEM results in Figs. 1 and 2). Actually, besides hollow grooves and molten-pool grooves, more diverse structures can be prepared by high-NA fs laser direct writing with a wider range of processing parameters or even circular polarization conditions, as shown in Figs. S1 and S4 in the supplementary information.

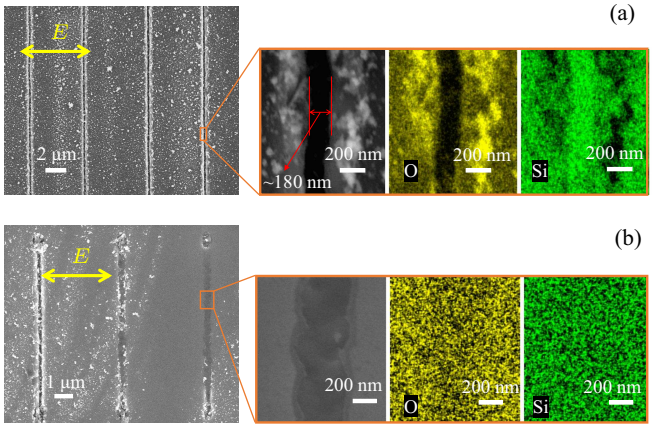


Fig. 3. SEM image and EDS composition analysis of (a) hollow single grooves and (b) molten-pool single grooves. The processing parameters of the two sets of results are as follows: (a) objective lens NA 0.95, pulse energy 1.24 nJ, scanning speed 10 μm·s^{-1}; (b) objective lens NA 0.95, pulse energy 1.00 nJ, scanning speed 5 μm·s^{-1} and processing of twice (left line: the hollow single groove), scanning speed 7 μm·s^{-1} and processing twice (middle line), scanning speed of 5 μm·s^{-1} and processing once (right line: the molten-pool single groove). The yellow and green maps on the right analysis charts are the O and Si component distribution maps from EDS measurements, respectively.

3.4. Influence of the relationship between laser polarization and scanning direction on the morphology of the single groove

As demonstrated above, the single nano-groove rooted in LSFL and related to laser–SPP interaction, is strongly polarization dependent. Here, the influence of the accurate angle relationship between laser polarization and scanning direction on the morphology of the single groove will be specifically explored. Under the processing conditions of NA 0.50, 10 μm·s^{-1} and 2.42 nJ, Fig. 4 displays three sets of single grooves of varying lengths with different polarization-scanning-direction angles. In Fig. 4(b), when the laser polarization is perpendicular to the scanning direction, the single groove can grow collimated along the scanning direction, thus becoming an extremely straight line: due to the polarization-dependent field enhancement and the multi-pulse incubation growth of the single nano-groove, it appears that the adverse effects of random vibration during processing will be significantly reduced, resulting in strong robustness of the linear

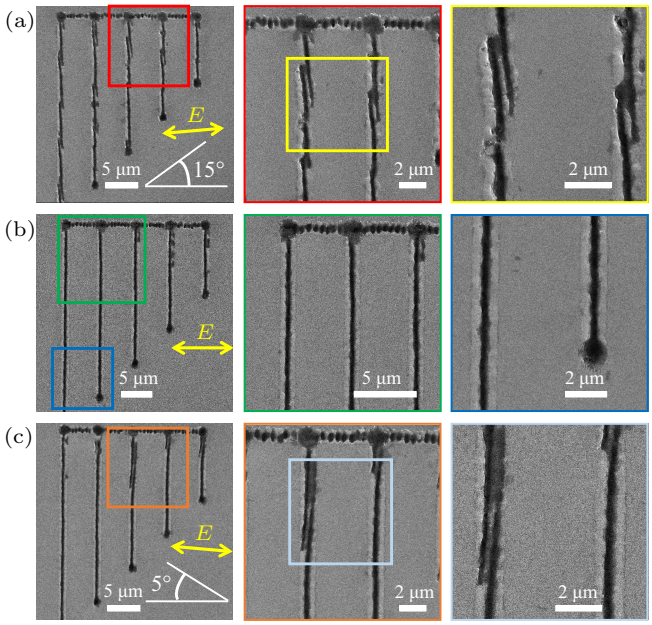


Fig. 4. Polarization-dependent morphological characteristics of single-groove structures prepared with the processing parameters of NA 0.50, 10 μm·s^{-1} and 2.42 nJ. Each vertical line is processed twice. The three sets of single grooves of varying length are prepared using different polarization-scanning-direction angles: (a) deflection angle of ∼ 15°; (b) deflection angle of ∼ 0°; (c) deflection angle of ∼ −5°. The different color boxes label the corresponding areas of the enlarged views shown on the right.

growth of the nano-groove. Then, a slightly deflected direction of laser polarization, as shown in Figs. 4(a) and 4(c) for deflection angles of 15° and 5°, respectively, may cause the single-groove structure to become a segment of the double-groove structure, even forming a kind of twisted structure in the case of large deflection angles. In fact, during nano-groove growth, the most prominent field enhancement occurs in the direction perpendicular to the polarization, which induces the groove to grow along the direction perpendicular to the polarization rather than the scanning direction. Thus, when the polarization is markedly deflected from the perpendicular direction of scanning, the direction of nano-groove growth will evidently deviate from the scanning direction, i.e., the main laser spot, which may lead to a new groove occurring in the main laser spot via the building-up or switching of field enhancement modes of two adjacent asymmetric nano-grooves.[7,12]

3.5. Composite nanostructure fabrication based on single nano-grooves

As a processing technique, in addition to parallel scanning processing the characteristics of interlaced processing are also worth special attention. In Fig. 5(a), the processing of single grooves is carried out in two orthogonal directions. Based on the pre-formed horizontal single grooves, the vertical grooves are prepared in two opposite directions to test the impact of preformed nano-grooves. As clearly shown in the enlarged SEM image, after scanning through the intersections, the occurrence of double grooves is highly possible due to the interference of pre-formed orthogonal grooves. It turns out that the pre-formed horizontal nano-groove may disturb the polarization-dependent field-enhanced feedback of the vertical single nano-groove and further act as a seed for the occurrence of field enhancement modes of double nano-grooves,[7,12] thus promoting the incubation growth of double nano-grooves, which will convert back to the more stable single nano-grooves in subsequent scanning. The mutual influence of this intersecting structure is a problem that still needs to be solved in actual processing.

In addition to the limited size of a single groove, the minimum processing spacing (period) that a composite structure can achieve is also an important factor in determining processing accuracy. In Fig. 5(b), parallel to the pre-formed single groove, further processing with a spacing of $\sim$ 200 nm or $\sim$ 300 nm is performed (this is smaller than the spatial period of LSFL). It can be observed that spacings of $\sim$ 200 nm or $\sim$ 300 nm are near the groove linewidth and the new groove can still be stably generated with a groove spacing of $\sim$ 500 nm or $\sim$ 600 nm (near the spatial period of LSFL), giving a structural processing accuracy of $\sim$ 500 nm. Furthermore, the processing stability of periodic structures based on a single groove is demonstrated in Fig. 5(c). When the scanning direction is perpendicular to the polarization, a periodic groove array with good uniformity and collimation can be prepared even though scanning is in two opposite directions. However, when the polarization has a small deflection angle of 3°, a defective groove array with twisted grooves may appear, which is prominent for only one scanning direction — the mechanism of such a non-reciprocal processing characteristic needs further research.

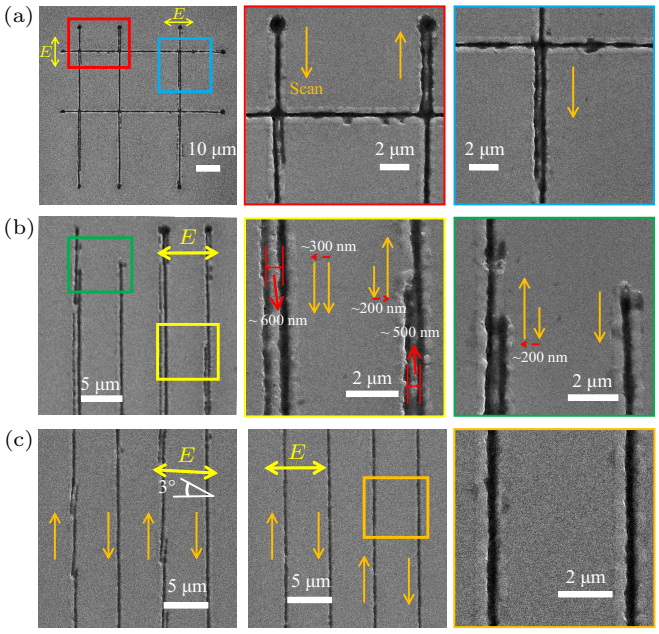


Fig. 5. Composite nanostructures fabrication based on single nano-grooves with the processing conditions NA 0.50, 10 μm·s^{-1} and 2.42 nJ. (a) Orthogonal single-groove structures with intersecting structures, the two horizontal grooves are prepared first, then the vertical grooves are processed in two opposite scanning directions, with a high possibility of forming double grooves after scanning through the intersections, as shown in the enlarged SEM figure on the right. (b) Parallel to a pre-formed single groove, another processing with a spacing of $\sim$ 200 nm (the first and fourth lines) or $\sim$ 300 nm (the third line) in two opposite scanning directions (the second line shows the original single groove) and the grooves with a spacing of $\sim$ 500 nm or $\sim$ 600 nm. The enlarged views on the right show the morphological details of parallel double grooves. (c) Periodic groove arrays with a 5 μm period prepared with a small deflection angle of 3° (the left defective array with twisted grooves) and without a deflection angle (the middle uniform array with good collimation). The enlarged view on the right shows the morphological details of the single grooves.

4. Conclusions

In short, by high-NA 800 nm fs laser direct writing with precise control of the pulse energy and scanning speed, polarization-dependent single grooves with a linewidth of $\sim$ 180 nm can be stably prepared on Si. Benefiting from the extraordinary field enhancement of polarization dependence in the nano-groove, the uniform single nano-groove can grow along an extremely straight line while resisting the impact of laser spot jitter during scanning processing. In addition, the single nano-groove can be efficiently deepened along with line-width clamping through different technical solutions. Based on the single nano-groove, multiple composite nanostructures can be flexibly prepared, for example a periodic groove array with good uniformity and collimation. The study

demonstrates that even on non-transparent Si, single nano-grooves derived from LIPSS can be robustly fabricated via single fs laser beam direct writing, resembling those on di-electrics. Therefore, preparation of single nano-grooves by fs laser direct writing may serve as a simple and flexible nano-processing technique on semiconductors.

Acknowledgements

Project supported by the Natural Science Foundation of Guangdong Province (Grant No. 2021A1515012335), the National Natural Science Foundation of China (Grant No. 11274400), Pearl River S&T Nova Program of Guangzhou (Grant No. 201506010059), State Key Laboratory of High Field Laser Physics (Shanghai Institute of Optics and Fine Mechanics), and State Key Laboratory of Optoelectronic Materials and Technologies (Sun Yat-Sen University).

References

[1] Cheng J, Liu C S, Shang S, Liu D, Perrie W, Dearden G and Watkins K 2013 *Opt. Laser Technol.* **46** 88
[2] Chichkov B N, Momma C, Nolte S, von Alvensleben F and Tünnermann A 1996 *Appl. Phys. A* **63** 109
[3] Momma C, Chichkov B N, Nolte S, von Alvensleben F, Tünnermann A, Welling H and Wellegehausen B 1996 *Opt. Commun.* **129** 134
[4] Hashida M, Mishima H, Tokita S and Sakabe S 2009 *Opt. Express* **17** 13116
[5] Liu Y, Ding Y, Xie J C, Xu L L, Wha Jeong I and Yang L J 2023 *Mater. Design* **225** 111443
[6] Birnbaum M 1965 *J. Appl. Phys.* **36** 3688
[7] Huang M and Xu Z Z 2014 *Laser Photonics Rev.* **8** 633
[8] Zhang H, Colombier J P and Witte S 2020 *Phys. Rev. B* **101** 245430
[9] Skolski J Z P, Römer G R B E, Obona J V, Ocelik V, Huis in 't Veld A J and De Hosson J T M 2012 *Phys. Rev. B* **85** 075320
[10] Bonse J and Gräf S 2020 *Laser Photonics Rev.* **14** 2000215
[11] Huang M, Zhao F L, Cheng Y, Xu N S and Xu Z Z 2009 *ACS Nano* **3** 4062
[12] Huang M, Cheng Y, Zhao F L and Xu Z Z 2013 *Ann. Phys. (Berl.)* **525** 74
[13] Shimotsuma Y, Kazansky P G, Qiu J R and Hirao K 2003 *Phys. Rev. Lett.* **91** 247405
[14] Sun X C, Liu X Q, Sun Z J, Li S X, Zheng J X, Xia H and Wang L 2022 *Opt. Express* **30** 32244
[15] Dusser B, Sagan Z, Soder H, Faure N, Colombier J P, Jourlin M and Audouard 2010 *Opt. Express* **18** 2913
[16] Taylor R, Hnatovsky C and Simova E 2008 *Laser Photonics Rev.* **2** 26
[17] Vorobyev A Y, Makin V S and Guo C 2009 *Phys. Rev. Lett.* **102** 234301
[18] Barberoglou M, Stratakis E, Zorba V, Spanakis E, Tzanetakis P, Anastasiadis S H and Fotakis C 2009 *CLEO/Europe - EQEC 2009 - European Conference on Lasers and Electro-Optics and the European Quantum Electronics Conference*, June 14–19, 2009, Munich, Germany, pp. 1–1
[19] Lopez-Santos C, Puerto D, Siegel J, Macias-Montero M, Florian C, Gil-Rostra J, Lopez-Flores V, Borras A, Gonzalez-Elipe A R and Solis J 2021 *Adv. Opt. Mater.* **9** 2001086
[20] Killaire G, Walia J, Rashid S, Berini P and Weck A 2022 *Appl. Surf. Sci.* **583** 152440
[21] Li R H, Zhou S N, Liu S T, Zhou Y H, Jiang S J and Huang M 2022 *Appl. Phys. A* **128** 1060
[22] Zhou S N, Li R H, Jiang S J and Huang M 2022 *Opt. Laser Technol.* **153** 108261
[23] Geng J, Yan W, Shi L P and Qiu M 2022 *Light Sci. Appl.* **11** 189
[24] Singh P C and Das S K 2021 *Pramana* **95** 11
[25] Huang J X, Xu K, Xu S L, Li X W 2022 *Laser Photonics Rev.* **16** 2200093
[26] Sarracino A, Ansari A W, Torralva B R and Yalisove S 2021 *Appl. Phys. Lett.* **118** 242106
[27] Liao Y, Cheng Y, Liu C N, Song J X, He F, Shen Y L, Chen D P, Xu Z Z, Fan Z C, Wei X B, Sugioka K and Midorikawa K 2013 *Lab Chip* **13** 1626
[28] Li Z Z, Wang L, Fan H, Yu Y H, Chen Q D, Juodkazis S and Sun H B 2020 *Light Sci. Appl.* **9** 41
[29] Yan Z, Gao J C, Beresna M and Zhang J Y 2022 *Adv. Opt. Mater.* **10** 2101676
[30] Tsibidis G D, Barberoglou M, Loukakos P A, Stratakis E and Fotakis C 2012 *Phys. Rev. B* **86** 115316
[31] Kelly R and Miotello A 1996 *Appl. Surf. Sci.* **96** 205
[32] Huang M, Zhao F L, Cheng Y, Xu N and Xu Z Z 2009 *Phys. Rev. B* **79** 125436
[33] Lin Z Y, Liu H G, Ji L F, Lin W X and Hong M H 2020 *Nano Lett.* **20** 4947
[34] Lin Z, Ji L and Hong M 2022 *Nano Lett.* **22** 7005